Internal tide coherence and decay over a wide shelf sea

Mark Inall,[1] Dmitry Aleynik,[1] Tim Boyd,[1] Matthew Palmer,[2] and Jonathan Sharples[2,3]

[1] A quasi-synoptic hydrography and velocity section is used to determine the structure and the decay rate of the internal tide (IT) across the broad continental shelf of the Celtic Sea. In these observations the IT is coherent over more than 170 km, about five wavelengths, with an estimated shoreward energy decay scale of 42 km. The inferred IT wavelength-averaged dissipation rate near the shelf edge is estimated as 2.08×10^{-7} Wkg^{-1}, in close agreement with tidally- and vertically-averaged measurements from the region. These results provide the first *in situ* evidence of IT coherence over many wavelengths in a shelf sea. **Citation:** Inall, M., D. Aleynik, T. Boyd, M. Palmer, and J. Sharples (2011), Internal tide coherence and decay over a wide shelf sea, *Geophys. Res. Lett.*, *38*, L23607, doi:10.1029/2011GL049943.

1. Introduction

[2] Internal waves are a major source of energy available to mix the stratified oceans. Tidal and near inertial internal waves form the most energetic part of the spectrum and the non-linear cascade of energy from the low frequency, long wavelength part of the spectrum fuels irreversible mixing at smaller scales. Vertical mixing mediated by internal tides (ITs) is an important part of the deep ocean buoyancy budget [*Munk and Wunsch*, 1998; *Sjoberg and Stigebrandt*, 1992], as well as ocean margin buoyancy and nutrient budgets [*Pingree and Mardell*, 1981; *Sharples et al.*, 2009]. With a fundamental wavelength of tens of kilometres ITs are easily modelled, and it follows that estimates of IT decay rate may offer a promising route to parameterising their effect on vertical mixing in shelf seas. Quantifying the IT decay rate has proven problematic because spatial coherence is difficult to demonstrate from spatially discrete measurements. Generalizing the IT decay rate is also problematic because decay rates are regionally specific, depending on stratification, water depth, bed roughness and local hydrodynamics. An IT parameterisation applicable to deep, supercritical ridges has been developed [*Klymak et al.*, 2010], however the decay rate of ITs and their effects on mixing the interior of shelf seas is uncertain. Remote sensing has shown IT energy to propagate coherently for many hundreds of kilometres across the Celtic Sea [*Pingree and New*, 1995]. Other studies have implied spatial coherence from spatially discrete observations: on the Malin Shelf [*Rippeth and Inall*, 2002; *Sherwin*, 1988]; on the Australian North West Shelf [*Holloway et al.*, 2001]; on the New Jersey Shelf [*Shroyer et al.*, 2010], and within fjordic systems [*Inall and Rippeth*, 2002]. Estimates of IT *e*-folding decay rate, though, are few: *Sherwin* [1988] gives a value of 85 km for the Malin Shelf, perhaps an over estimate [*Inall et al.*, 2000]; *Craig* [1991] estimated IT decay scale dependence on internal and bed-induced friction; and an estimate of 35 km was derived for the New Jersey shelf [*Shroyer et al.*, 2010]. Furthermore, evidence has mounted that the decay of internal wave energy is approximately equal to the measured dissipation rate [*Inall and Rippeth*, 2002; *Moum et al.*, 2007; *Shroyer et al.*, 2010]. Although IT decay scales in shelf seas have some regional dependency, developing greater knowledge of the decay scale is a key step towards developing parameterizations. This is a critical development since the dissipative processes are expected to remain sub-grid scale in shelf sea numerical models for the foreseeable future. In this paper, a quasi-synoptic hydrography and velocity section is used to estimate the horizontal structure and the decay rate of the IT across the broad shelf of the Celtic Sea, and the dissipation rate inferred from this decay rate is compared to direct measurements from the region.

2. Observations and Instrumentation

[3] An undulator (Scanfish), equipped with a Seabird 911 CTD and towed at 4.4 ms^{-1} was profiled from 5 m below the surface to 10 m above the bed along the 250 km section "TR1" (Figure 1), taking 16.3 hours to complete on 25th/26th July 2008. Cycling every 2 minutes gave an effective horizontal resolution of 260 m. The following coordinate system is adopted: x and y (and u and v) are defined along and across section, with $x = 40$ km at the shelf break (180 m isobath), y is positive northward, and z is positive downwards. Data were gridded onto an xz-plane using linear distance weighting, with $\Delta x = 750$ m, $\Delta z = 2$ m and search radii $sx = 500$ m and $sz = 4$ m. A 150 kHz hull-mounted Acoustic Doppler Current Profiler (ADCP) returned profiles of absolute horizontal velocities in 4 m bins averaged into 2-minute ensembles, from 14 m below surface to 15 m above bottom. Velocities were gridded in an identical fashion to the CTD data. Section TR1 ended at Jones Bank, an isolated topographic feature extending 25 km in the SW-NE direction and 11 km across, rising 45 m above surrounding shelf (Figure 1). To account for the unintentional dog-leg in the cruise track data locations for the dog-leg segment were projected onto a straight across-slope transect, introducing a weak local temporal compression of the observations in the spatial reference frame.

3. Analysis

[4] Stratification varied from a diffuse vertical structure at the shelf break to a tight pycnocline centred on 35 m over Jones Bank (Figure 2a). Vertical perturbations were

[1]Scottish Association for Marine Science, Oban, UK.
[2]National Oceanography Centre, Liverpool, UK.
[3]School of Environmental Sciences, University of Liverpool, Liverpool, UK.
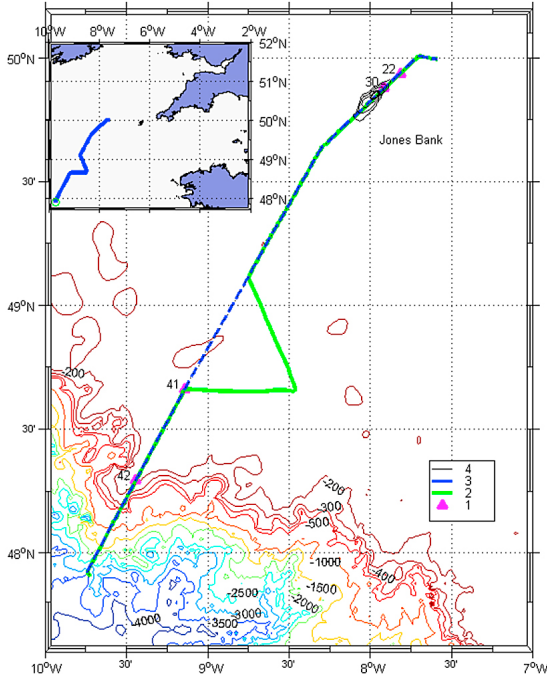
Figure 1. Bathymetry of the Celtic sea area (Etopo1) and CTD stations (triangles, 1). RRS James Cook ship track with Scanfish section TR1 from shelf break to Jones Bank (green line, 2). Section geometrically adjusted assuming long wavelength internal tide propagating with phase lines parallel to shelf break (blue dashed line, 3). Jones Bank bathymetric contours at 10 m intervals from 80 m to 110 m (black line, 4).

present at a range of scales, with a dominant quasi-periodic perturbation the $\sigma_\theta = 26.5$ isopycnal, amplitude 10 to 15 m, and a wavelength of about 35 km. The spectrum of the displacement anomaly of the $\sigma_\theta = 26.5$ kg·m^{-3} isopycnal has its largest peak at 41 km (Figure 3). If this peak corresponds to a propagating baroclinic signal, then it will be Doppler shifted by the relative velocity of the ship to the wave phase speed. The former is known (4.4 ms^{-1}) and the latter computed using the internal wave vertical structure equation, which gives a wavelength of 35 km and phase speed of $C_p = 0.78$ ms^{-1} for the fundamental M2 internal tide (using the mid-shelf density structure, Station 41, Figure 1). The Doppler-corrected wavelength is 33.5 km, very close to the dynamical mode estimate (35 km), strongly suggesting the spectral peak in pycnocline perturbations is associated with a low mode IT propagating throughout section TR1. Alternatively it is possible that the pycnocline perturbations were locally generated by topography. The ADCP data are used to distinguish between local versus remote generation: remote generation demands a fixed phase relationship between velocity and amplitude of a propagating IT. Since the tow speed is approximately 6 times faster than the mode 1 phase speed, a mode 1 wave appears nearly stationary to the moving vessel (16% Doppler red-shift). Baroclinic velocity profiles are first defined: $u'(z,x) = u(z,x) - \langle u \rangle_z$, where $u(z,x)$ are the measured velocity profiles and $\langle u \rangle_z$ the vertically averaged (barotropic) velocities, similarly for v. From $x = 50$ to 160 km a very clear beam-like V-shaped structure is

apparent in $u'(z,x)$ (Figure 2b). Farther from the shelf break, from $x = 160$ to 245 km, a less pronounced signal is evident. Such structure in the baroclinic velocity field is highly reminiscent of energy propagating along ray paths and a very strong indicator of the on-shore energy propagation of a spatially coherent IT. The ray-like features in $u'(z,x)$ are compared with the theoretical trajectory of M2 internal wave energy. In a stationary, stratified medium internal wave energy propagates at an angle α to the horizontal, given by:

$$\alpha = \frac{\left(\omega - \langle u \rangle_z(x) \cdot k\right)^2 - f^2}{N^2 - \left(\omega - \langle u \rangle_z(x) \cdot k\right)^2} \quad (1)$$

In which ω is the M2 tidal frequency, f the Coriolis parameter, N the stratification parameter, and k the horizontal wavenumber of the mode 1 IT ($k = 2\pi/33.5 \times 10^3$ m). The $\langle u \rangle_z(x) \cdot k$ term accounts for the advective effect of the barotropic tide in modifying the apparent frequency of the IT. Given an initial starting point and propagation direction rays traced according to equation (1) in are superimposed on the velocity structure observed over the shelf (Figure 2b). Two separate ray paths are shown: Ray 1, starting above the shelf break ($x = 52$ km and $z = 30$ m), and Ray 2, starting above the flank of Jones Bank ($x = 195$ km and $z = 30$ m).

4. Linear Generation and Energetics

[5] We have shown how the longest baroclinic wave response of the shelf break to barotropic tidal forcing propagates in a coherent, planar fashion from the break and across the shelf. Pursuing a 2-dimensional approach we evaluate the IT-generating vertical body force (over a tidal period), which can be expressed as [*Baines*, 1982]:

$$F(x) = \frac{Q}{\omega} \frac{h'(x)}{h(x)^2} \int_0^h N^2(x,z) z \partial z \quad (2)$$

In which Q is the tidal volume flux, and h the total water depth. $F(x)$ is computed using observed stratification, bathymetry, and tidal forcing. Since $F(x)$ represents the forcing term of the internal wave equation, and of interest here is the lowest mode response, it is reasonable to smooth $h'(x)$, the seabed slope, with a 33 km low-pass filter (Figure 2c). $F(x)$ has a maximum at the shelf break, exceeding values elsewhere by more than a factor of 6. A secondary peak in $F(x)$ is evident at $x = 250$ km (Jones Bank). The 2D approach assumes that topography is a continuous barrier to the cross-shelf flow. Since the topographic features on the shelf (at $x = 135$ km, and $x = 250$ km) have limited across-section extent, and their potential as planar wave generators will be exaggerated by equation (2). Nevertheless Figure 2c serves to reinforce the notion that the shelf break dominates IT generation in this region. It is important to also account for time variation in equation (1). The snapshot of five IT wavelengths correspond to a little under three days of forcing conditions at the shelf break, during which time the magnitude of the modelled cross-shelf barotropic tide at the shelf break decreased from 0.37 ms^{-1} to 0.29 ms^{-1} [*Wakelin et al.*, 2009]. This change in the tide,
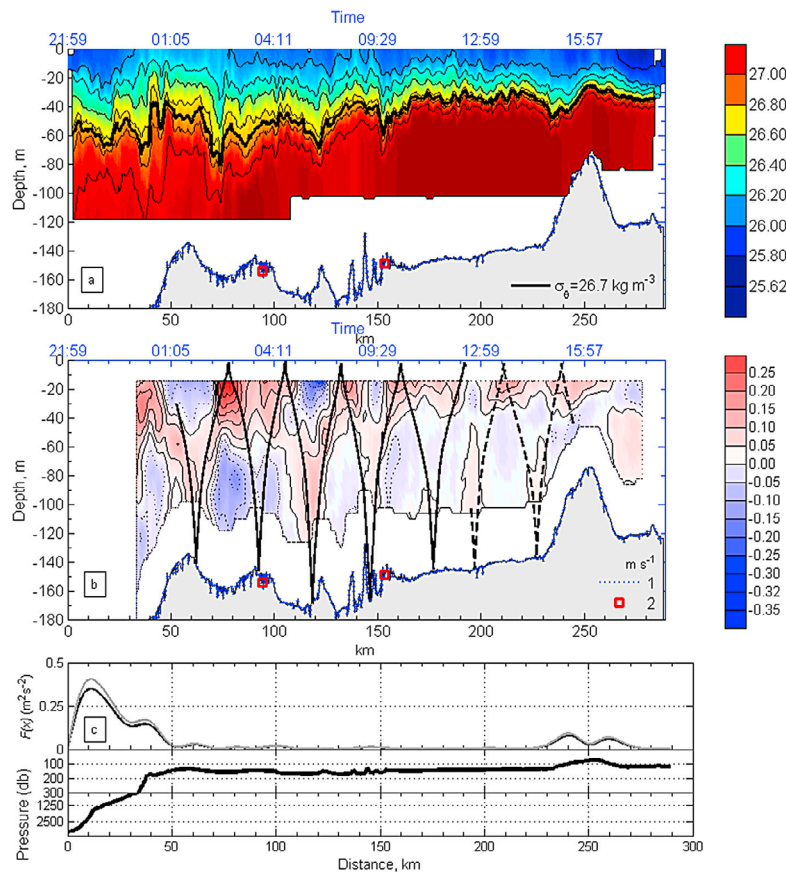
Figure 2. (a) σ_θ along section TR1 as a function of distance from shelf break along the blue line of Figure 1. Search radii sz = 4 m, sx = 0.5 km, and grid dx = 0.75 km, dz = 2 m. (b) Vertical distribution of the along-section baroclinic velocity. Superimposed are the Doppler shifted theoretical ray traces for an M2 period internal wave. (c) Vertically integrated internal tide forcing potential, after *Baines* [1982], as described in the text, and bathymetry profile; note the split scale for bathymetry. Grey and black lines indicate the range over the 3 day "age" of the baroclinic tide.
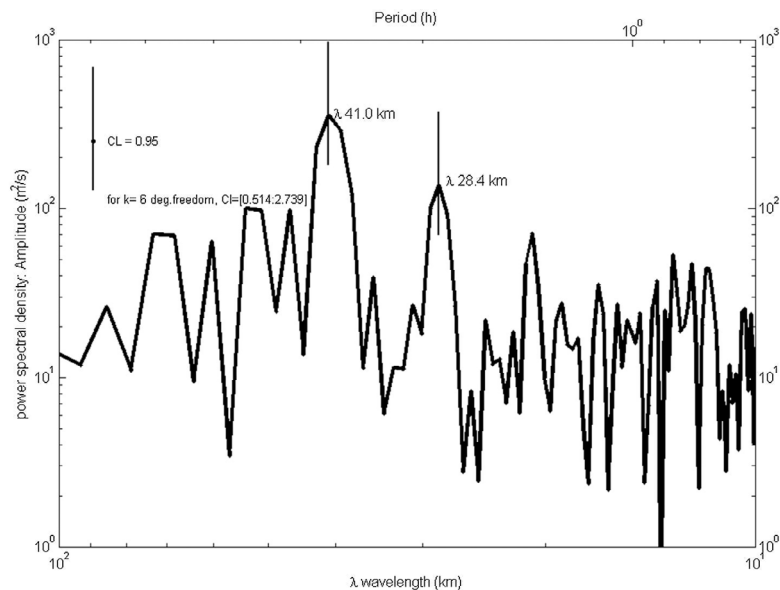

Figure 3. Spectrum of $\sigma_\theta = 26.5$ kg•m^{-3} depth anomaly in a frequency and wavenumber domains, 95% confidence interval shown for main frequencies calculated using six degrees of freedom (estimated using the fast fourier transform of the auto-correlation function of de-trended 1024 data-point intervals, a half-size Hanning window, and normalized with respect to wavenumber).
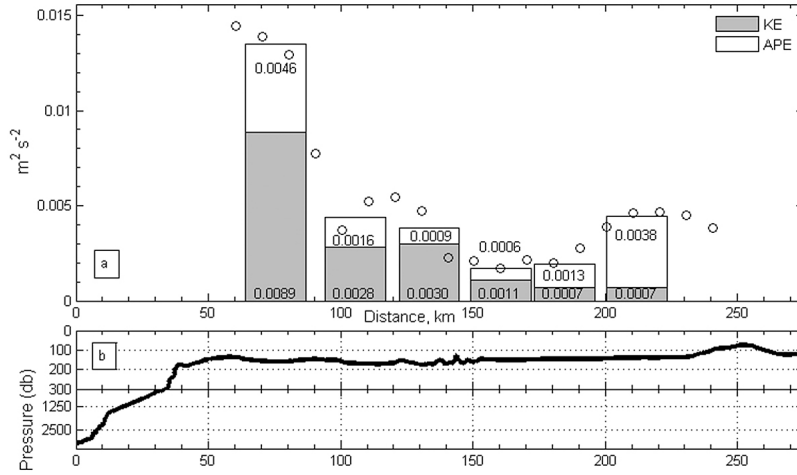
Figure 4. (a) Depth and unit-wavelength averaged values of KE and APE over six internal tide wavelengths, $m^2 s^{-2}$ (bars), running unit-wavelength averages of the total energy shown every 5 km (open circles), and (b) bathymetry profile.

$Q(t)$, translates proportionately into $F(x)$ (equation (2) and Figure 2c), and quadratically into the energy density of the IT: its effects are incorporated with a scaling, $S(x)$, factor below.

[6] We estimate the total baroclinic energy density distribution broadly following the methodology of *Althaus et al.* [2003]. The spatial series of baroclinic velocity profiles was divided into six segments ($\lambda = 1$ to 6), each corresponding to one IT wavelength as defined by the ray paths, and averages of over each wavelength computed ($\langle u'(z,\lambda)\rangle_x$, $\langle v'(z,\lambda)\rangle_x$). The baroclinic perturbation velocity is therefore $\tilde{u}(z,x) = u'(z,x) - \langle u'(z,\lambda)\rangle_x$. For each segment ($\lambda = 1$ to 6) we compute an average, or reference, potential density vertical profile and define the depth of each iospycnal in the reference profile as $\langle z(\sigma_\theta,\lambda)\rangle_x$. We subtract the depth of each isopycnal from the depth of the same isopycnal in the reference profile to give the isopycnal displacement profiles $\xi(\sigma_\theta,x) = z(\sigma_\theta,x) - \langle z(\sigma_\theta,\lambda)\rangle_x$. The displacement, ξ, varied from 40 to 50 m over the shelf-break for the deepest isopycnals ($\sigma_\theta = 26.8$–27.0 kgm^{-3}) to $\pm$ few meters on the inner part of the Celtic sea shelf. Baroclinc energy density (kinetic plus available potential) for each segment is:

$$E(\lambda, z) = KE + APE = 0.5\rho_0 \left\langle \tilde{u}^2 + \tilde{v}^2 + \overline{N}^2 \xi^2 \right\rangle_\lambda \quad (3)$$

In which wavelength averaging is denoted by $\langle \rangle_\lambda$. To allow for a comparative spatial analysis, $\overline{E(\lambda)}$ is scaled by a factor $S(x) = (Q(t_0)/Q(t))^2$ to account of the change in barotropic forcing with time, where t_0 is the start time of section TR1, and $t = x/C_p$ is the "age" of the baroclinic tide. $S(x)$ is derived from windowed harmonic analyses of the M2 amplitude of modelled cross-slope currents at the shelf break [*Wakelin et al.*, 2009], and varies nearly linearly from one at $\lambda = 1$ to $S(x) = 0.62$ at $\lambda = 6$. $S(x)$ is not applied beyond $\lambda = 5$, due to the influence of Jones Bank.

[7] The distribution of depth averaged *KE* and *APE* densities along the section ($\overline{E(\lambda)}$ for $\lambda = 1$ to 6) are shown in Figure 4. Independent one-wavelength averages and running

unit-wavelength averages are shown. The largest (scaled) baroclinic energy density, $\overline{E(\lambda)}$, occurs closest to the shelf-break (centred on $x = 75$ km) with a value of 0.0135 $m^2 s^{-2}$ (13.9 Jm^{-3}). Relatively high values of E are also found over the slopes of Jones Bank (0.0045 $m^2 s^{-2}$ or 4.6 Jm^{-3}), mainly associated with *APE* in that case. The dip at $x = 100$ km is associated solely with a local dip in calculated *APE*. An exponential fit ($R = 0.95$) to the first five independent values for $\overline{E(\lambda)}$ gives an *e*-fold scale of $b_\lambda = 42$ km.

5. Discussion

[8] Several assumptions and simplifications have necessarily been made in using a single shelf-wide section of density and velocity structure to estimate the decay length scale of the IT, and yet a consistent story has emerged. Since there is only a single realisation of section TR1 it is not possible to place error bars on the estimate of b_λ. Two consistency checks are possible: firstly by comparing the IT energy flux to the directly computed baroclinic energy flux; and secondly by comparing the IT energy flux divergence to the turbulent kinetic energy dissipation. IT energy flux can be expressed as the product of the energy density and group speed, $E_f = \overline{E} \cdot C_g$, where the group velocity, $Cg = 0.78$ ms^{-1}. For example the on-shelf flux at $\lambda = 1$ is $E_f = 1.59$ kWm^{-1}. Following *Kunze et al.* [2002] and using baroclinic velocities and isopycnal displacement perturbations as defined above, direct depth averaged baroclinic energy flux estimates were made, giving $E_{fD} = 0.94$ kWm^{-1} at $\lambda = 1$ and $E_{fD} = -0.031$ Wm^{-1} at Jones Bank, further reinforcing the notion of shoreward propagating energy across the shelf, with a sign reversal in the vicinity of Jones Bank.

[9] The second comparison is between the energy flux divergence, ΔE_f, and directly measured dissipation. Assuming the energy lost is dissipated locally, we estimate the average dissipation rate per unit mass over one wavelength of the tide as $D = \Delta E_f/H\lambda$, where $H = 147$ m is the mean water depth across the shelf; giving an average dissipation rate between $x = 75$ km and $x = 110$ km of $D = 2.08 \times 10^{-7}$ Wkg^{-1}. An equivalent figure for the (much less

energetic) Malin Shelf is 7.1×10^{-9} Wkg^{-1} (using data from *Sherwin* [1988]), which has been compared to direct dissipation measurements made near the Malin Shelf break (tidal and depth average) of 1.8×10^{-8} Wkg^{-1} [*Inall et al.*, 2000]. An explanation for the higher value of the direct measure is that it was made close to the shelf break, whilst the lower inferred measure is effectively a spatial average over one IT wavelength. Direct dissipation measurements have also been made near the Celtic Sea shelf break, Figure 9a of *Sharples et al.* [2009] (which should show units of Wm^{-3} rather than Wkg^{-1}). Using their original data an appropriately tidally and vertically averaged value for dissipation is 2.15×10^{-7} Wkg^{-1}, remarkably close the wavelength-average inferred value of $D = 2.08 \times 10^{-7}$ Wkg^{-1}. The direct dissipation measurements were made at neaps, and at the more energetic end of our one-wavelength averaging interval. Such close agreement between the two energy loss estimates is likely a fortuitous combination of these two counter-balancing effects. Considering all these factors, the value estimated here of $D = 2.08 \times 10^{-7}$ Wkg^{-1} is highly plausible.

[10] Assuming that energy decay is balanced by dissipative loss, a decay scale over other continental shelves can be derived from other published studies, for example the observations of *MacKinnon and Gregg* [2003] for which an onshore flux of 130 Wm^{-1} was dissipated at a rate of 5 to 50×10^{-9} Wkg^{-1} in 70 m of water over the New England shelf, yields an (*e*-folding) decay scale of between 23 and 230 km. A more precise estimate of 35 km is derived for the New Jersey shelf from observations of *Shroyer et al.* [2010]. They suggest that the internal tide off the New Jersey shelf moves energy from an internal bore-like feature into non-linear internal wave (NLIW) packets over a near-field region around the shelf edge, and that shoreward of this region of wave growth, the NLIW packets decay at a rate that is approximately equal to the observed dissipation rate. The observations discussed here present a different picture: away from the near-field generation region, the energy in the linear internal tide is observed to decay shoreward of the shelf break at a rate that is consistent with previous tidally averaged dissipation measurements. The crucial difference between these views is that the analysis of the present observations implies that the linear internal tide continually feeds energy into shorter wavelength features [e.g., *Gerkema*, 1996] which mediate the transfer of energy to the dissipative processes over the shelf.

[11] Previous studies in this region [*Green et al.*, 2008] concluded that little shelf break-generated IT energy was available for mixing at a distance of 180 km from the shelf break ($x = 220$ km in our coordinate system). The results presented here are consistent with that result, however *Green et al.* [2008] also concluded that little energy propagates inshore of the shelf break in contrast to the analysis presented here. Their measurements, made at the shelf break (Station 42, Figure 1), are in the complex nearfield of the wave generation zone and are confounded by a mixture of locally dissipating high frequency waves and the long-wave IT response, which will not be fully developed so close to the generation zone. Viewing the low mode IT at order 10s of km away from the generation zone after it has emerged from the complexity of the generation region allows for a clearer view of the long semi-diurnal IT and its cross-shelf

decay. Whilst sea surface signature of the IT has been observed as a coherent feature over 100's of km in the open ocean [*Ray and Mitchum*, 1996] and shelf seas [*Pingree and New*, 1995], here we have demonstrated *in situ* spatial coherence and quantified the baroclinic structure of the IT propagating 170 km shoreward across a wide shelf sea.

References

Althaus, A. M., E. Kunze, and T. B. Sanford (2003), Internal tide radiation from Mendocino Escarpment, *J. Phys. Oceanogr.*, 33, 1510–1527, doi:10.1175/1520-0485(2003)033<1510:ITRFME>2.0.CO;2.

Baines, P. G. (1982), On internal tide generation models, *Deep Sea Res., Part A*, 29(3), 307–338, doi:10.1016/0198-0149(82)90098-X.

Craig, P. D. (1991), Incorporation of damping into internal wave models, *Cont. Shelf Res.*, 11(6), 563–577, doi:10.1016/0278-4343(91)90011-T.

Gerkema, T. (1996), A unified model for the generation and fission of internal tides in a rotating ocean, *J. Mar. Res.*, 54(3), 421–450, doi:10.1357/0022240963213574.

Green, J. A. M., J. H. Simpson, S. Legg, and M. R. Palmer (2008), Internal waves, baroclinic energy fluxes and mixing at the European shelf edge, *Cont. Shelf Res.*, 28(7), 937–950, doi:10.1016/j.csr.2008.01.014.

Holloway, P. E., P. G. Chatwin, and P. Craig (2001), Internal tide observations from the Australian North West Shelf in summer 1995, *J. Phys. Oceanogr.*, 31(5), 1182–1199, doi:10.1175/1520-0485(2001)031<1182:ITOFTA>2.0.CO;2.

Inall, M. E., and T. P. Rippeth (2002), Dissipation of tidal energy and associated mixing in a wide fjord, *Environ. Fluid Mech.*, 2, 219–240, doi:10.1023/A:1019846829875.

Inall, M. E., T. P. Rippeth, and T. J. Sherwin (2000), Impact of non-linear waves on the dissipation of internal tidal energy at a shelf break, *J. Geophys. Res.*, 105(C4), 8687–8705, doi:10.1029/1999JC900299.

Klymak, J. M., S. Legg, and R. Pinkel (2010), A simple parameterisation of turbulent tidal mixing near supercritical topography, *J. Phys. Oceanogr.*, 40, 2059–2074, doi:10.1175/2010JPO4396.1.

Kunze, E., L. K. Rosenfield, G. S. Carter, and M. C. Gregg (2002), Internal waves in Monterey Submarine Canyon, *J. Phys. Oceanogr.*, 32, 1890–1913, doi:10.1175/1520-0485(2002)032<1890:IWIMSC>2.0.CO;2.

MacKinnon, J. A., and M. C. Gregg (2003), Mixing on the late-summer New England Shelf—Solibores, shear, and stratification, *J. Phys. Oceanogr.*, 33, 1476–1492, doi:10.1175/1520-0485(2003)033<1476:MOTLNE>2.0.CO;2.

Moum, J. N., D. M. Farmer, E. L. Shroyer, W. D. Smyth, and L. Armi (2007), Dissipative losses in nonlinear internal waves propagating across the continental shelf, *J. Phys. Oceanogr.*, 37, 1989–1995, doi:10.1175/JPO3091.1.

Munk, W., and C. Wunsch (1998), Abyssal recipes II: Energetics of tidal and wind mixing, *Deep Sea Res., Part I*, 45, 1977–2010, doi:10.1016/S0967-0637(98)00070-3.

Pingree, R. D., and G. T. Mardell (1981), Slope turbulence, internal waves and phytoplankton growth at the Celtic Sea shelf-break, *Philos. Trans. R. Soc. A*, 302(1472), 663–682, doi:10.1098/rsta.1981.0191.

Pingree, R. D., and A. L. New (1995), Structure, seasonal development and sunglint spatial coherence of the internal tide on the Celtic and Armorican Shelves in the Bay of Biscay, *Deep Sea Res., Part I*, 42(2), 245–284, doi:10.1016/0967-0637(94)00041-P.

Ray, R. D., and G. T. Mitchum (1996), Surface manifestation of internal tides generated near Hawaii, *Geophys. Res. Lett.*, 23, 2101–2104, doi:10.1029/96GL02050.

Rippeth, T. P., and M. E. Inall (2002), Observations of the internal tide and associated mixing across the Malin Shelf, *J. Geophys. Res.*, 107(C4), 3028, doi:10.1029/2000JC000761.

Sharples, J., C. M. Moore, A. E. Hickman, P. M. Holligan, J. F. Tweddle, M. R. Palmer, and J. H. Simpson (2009), Internal tidal mixing as a control on continental margin ecosystems, *Geophys. Res. Lett.*, 36, L23603, doi:10.1029/2009GL040683.

Sherwin, T. J. (1988), Analysis of an internal tide observed on the Malin Shelf, north of Ireland, *J. Phys. Oceanogr.*, 18, 1035–1050, doi:10.1175/1520-0485(1988)018<1035:AOAITO>2.0.CO;2.

Shroyer, E. L., J. N. Moum, and J. D. Nash (2010), Energy transformations and dissipation of nonlinear internal waves over New Jersey's continental

shelf, *Nonlinear Processes Geophys.*, *17*(4), 345–360, doi:10.5194/npg-17-345-2010.

Sjoberg, B., and A. Stigebrandt (1992), Computations of the geographical-distribution of the energy flux to mixing processes via internal tides and the associated vertical circulation in the ocean, *Deep Sea Res., Part A*, *39*(2), 269–291, doi:10.1016/0198-0149(92)90109-7.

Wakelin, S. L., J. T. Holt, and R. Proctor (2009), The influence of initial conditions and open boundary conditions on shelf circulation in a 3D ocean-shelf model of the north east Atlantic, *Ocean Dyn.*, *59*, 67–81, doi:10.1007/s10236-008-0164-3.

D. Aleynik, T. Boyd, and M. Inall, Scottish Association for Marine Science, Oban PA37 1QA, UK. (mei@sams.ac.uk)

M. Palmer and J. Sharples, National Oceanography Centre, 6 Brownlow Street, Liverpool L3 5DA, UK.